duplicates were deleted to obtain predictions on the dispensability of the underlying enzymatic reaction.

Comparison of *Mycoplasma* and *Saccharomyces* genomes

We calculated the frequency of non-essential genes in the *M. genitalium* and the *S. cerevisiae* genomes (only single-copy genes were considered). Gene duplicates were identified using a BLAST protein search, with at least 25% amino acid similarity (using different thresholds do not affect our results). The list of putative essential *Mycoplasma* genes is from ref. 26. We found 1,881 out of 3,003 single-copy yeast genes that are non-essential. This figure is 83 out of 356 genes for *Mycoplasma*.

Received 14 January; accepted 30 April 2004; doi:10.1038/nature02636.

1. Giaever, G. *et al.* Functional profiling of the *Saccharomyces cerevisiae* genome. *Nature* **418,** 387–391 (2002).
2. Forster, J., Famili, I., Fu, P., Palsson, B. O. & Nielsen, J. Genome-scale reconstruction of the *Saccharomyces cerevisiae* metabolic network. *Genome Res.* **13,** 244–253 (2003).
3. Famili, I., Forster, J., Nielsen, J. & Palsson, B. O. *Saccharomyces cerevisiae* phenotypes can be predicted by using constraint-based analysis of a genome-scale reconstructed metabolic network. *Proc. Natl Acad. Sci. USA* **100,** 13134–13139 (2003).
4. Forster, J., Famili, I., Palsson, B. O. & Nielsen, J. Large-scale evaluation of *in silico* gene deletions in *Saccharomyces cerevisiae*. *OMICS* **7,** 193–202 (2003).
5. Segre, D., Vitkup, D. & Church, G. M. Analysis of optimality in natural and perturbed metabolic networks. *Proc. Natl Acad. Sci. USA* **99,** 15112–15117 (2002).
6. Steinmetz, L. M. *et al.* Systematic screen for human disease genes in yeast. *Nature Genet.* **31,** 400–404 (2002).
7. Wagner, A. Robustness against mutations in genetic networks of yeast. *Nature Genet.* **24,** 355–361 (2000).
8. Gu, Z. *et al.* Role of duplicate genes in genetic robustness against null mutations. *Nature* **421,** 63–66 (2003).
9. Gu, X. Evolution of duplicate genes versus genetic robustness against null mutations. *Trends Genet.* **19,** 354–356 (2003).
10. Stelling, J., Klamt, S., Bettenbrock, K., Schuster, S. & Gilles, E. D. Metabolic network structure determines key aspects of functionality and regulation. *Nature* **420,** 190–193 (2002).
11. Papin, J. A., Price, N. D., Wiback, S. J., Fell, D. A. & Palsson, B. O. Metabolic pathways in the post-genome era. *Trends Biochem. Sci.* **28,** 250–258 (2003).
12. Emmerling, M. *et al.* Metabolic flux responses to pyruvate kinase knockout in Escherichia coli. *J. Bacteriol.* **184,** 152–164 (2002).
13. Kitami, T. & Nadeau, J. H. Biochemical networking contributes more to genetic buffering in human and mouse metabolic pathways than does gene duplication. *Nature Genet.* **32,** 191–194 (2002).
14. Pál, C., Papp, B. & Hurst, L. D. Rate of evolution and gene dispensability. *Nature* **421,** 496–497 (2003).
15. Thatcher, J. W., Shaw, J. M. & Dickinson, W. J. Marginal fitness contributions of nonessential genes in yeast. *Proc. Natl Acad. Sci. USA* **95,** 253–257 (1998).
16. Edwards, J. S. & Palsson, B. O. The *Escherichia coli* MG1655 *in silico* metabolic genotype: its definition, characteristics, and capabilities. *Proc. Natl Acad. Sci. USA* **97,** 5528–5533 (2000).
17. Daran-Lapujade, P. *et al.* Role of transcriptional regulation in controlling fluxes in central carbon metabolism of *Saccharomyces cerevisiae*: a chemostat culture study. *J. Biol. Chem.* **279,** 9125–9138 (2004).
18. Nakao, M. *et al.* Genome-scale gene expression analysis and pathway reconstruction in KEGG. *Genome Inform. Ser. Workshop Genome Inform.* **10,** 94–103 (1999).
19. Schilling, C. H., Edwards, J. S., Letscher, D. & Palsson, B. O. Combining pathway analysis with flux balance analysis for the comprehensive study of metabolic systems. *Biotechnol. Bioeng.* **71,** 286–306 (2000).
20. Wagner, G. P., Booth, G. & Bagheri-Chaichian, H. A population genetic theory of canalization. *Evolution* **51,** 329–347 (2000).
21. Seoighe, C. & Wolfe, K. H. Yeast genome evolution in the post-genome era. *Curr. Opin. Microbiol.* **2,** 548–554 (1999).
22. Papp, B., Pal, C. & Hurst, L. D. Dosage sensitivity and the evolution of gene families in yeast. *Nature* **424,** 194–197 (2003).
23. Gerdes, S. Y. *et al.* Experimental determination and system level analysis of essential genes in *Escherichia coli* MG1655. *J. Bacteriol.* **185,** 5673–5684 (2003).
24. Kobayashi, K. *et al.* Essential *Bacillus subtilis* genes. *Proc. Natl Acad. Sci. USA* **100,** 4678–4683 (2003).
25. Kamath, R. S. *et al.* Systematic functional analysis of the *Caenorhabditis elegans* genome using RNAi. *Nature* **421,** 231–237 (2003).
26. Hutchison, C. A. *et al.* Global transposon mutagenesis and a minimal *Mycoplasma* genome. *Science* **286,** 2165–2169 (1999).
27. Glasner, J. D. *et al.* ASAP, a systematic annotation package for community analysis of genomes. *Nucleic Acids Res.* **31,** 147–151 (2003).
28. Altschul, S. F. *et al.* Gapped BLAST and PSI-BLAST: a new generation of protein database search programs. *Nucleic Acids Res.* **25,** 3389–3402 (1997).
29. Mewes, H. W. *et al.* MIPS: a database for genomes and protein sequences. *Nucleic Acids Res.* **30,** 31–34 (2002).

Supplementary Information accompanies the paper on **www.nature.com/nature**.

Acknowledgements We thank J. Förster and B. Palsson for discussions and providing information on the yeast flux balance model. We also thank J. Glasner for providing growth data on the *E. coli* wild-type strain. B.P. and C.P. were supported by the Hungarian National Research Grant Foundation (OTKA).

Competing interests statement The authors declare that they have no competing financial interests.

Correspondence and requests for materials should be addressed to L.D.H. (l.d.hurst@bath.ac.uk).

Temporal difference models describe higher-order learning in humans

Ben Seymour[1], John P. O'Doherty[1], Peter Dayan[2], Martin Koltzenburg[3], Anthony K. Jones[4], Raymond J. Dolan[1], Karl J. Friston[1] & Richard S. Frackowiak[1,5]

[1]*Wellcome Department of Imaging Neuroscience, 12 Queen Square, London WC1N 3BG, UK*
[2]*Gatsby Computational Neuroscience Unit, Alexandra House, 17 Queen Square, London WC1N 3AR, UK*
[3]*Institute of Child Health, University College London, 30 Guilford St, London WC1N 1EH, UK*
[4]*University of Manchester Rheumatic Diseases Centre, Hope Hospital, Manchester M6 8HD, UK*
[5]*Fondazione Santa Lucia, 00179 Rome, Italy*

The ability to use environmental stimuli to predict impending harm is critical for survival. Such predictions should be available as early as they are reliable. In pavlovian conditioning, chains of successively earlier predictors are studied in terms of higher-order relationships, and have inspired computational theories such as temporal difference learning[1]. However, there is at present no adequate neurobiological account of how this learning occurs. Here, in a functional magnetic resonance imaging (fMRI) study of higher-order aversive conditioning, we describe a key computational strategy that humans use to learn predictions about pain. We show that neural activity in the ventral striatum and the anterior insula displays a marked correspondence to the signals for sequential learning predicted by temporal difference models. This result reveals a flexible aversive learning process ideally suited to the changing and uncertain nature of real-world environments. Taken with existing data on reward learning[2], our results suggest a critical role for the ventral striatum in integrating complex appetitive and aversive predictions to coordinate behaviour.

Substantial evidence in humans and other animals has outlined a network of brain regions involved in the prediction of painful and aversive events[3–6]. Most of this work has concentrated on its simplest realization, namely first-order pavlovian fear conditioning; however, the predictions in this paradigm are rudimentary, showing little of the complexities associated with sequences of predictors that are critical in psychological investigations of prognostication[7]. These latter studies led to a computational account called temporal difference learning[1,8], which has close links with methods for prediction, and optimal action selection, in engineering[9]. When applied to first-order appetitive conditioning, temporal difference learning provides a compelling account of neurophysiological data, both with respect to the phasic activity of dopamine neurons in animal studies, and with blood-oxygenation-level-dependent (BOLD) activity in human functional neuroimaging studies[10–15]. However, beyond this simple paradigm, the utility of temporal difference models to describe learning remains largely unexplored. Here we provide a neurobiological investigation based on aversive and, importantly, sequential conditioning.

We used fMRI to investigate the pattern of brain responses in humans during a second-order pain learning task. Fourteen healthy subjects were shown two visual cues in succession, followed by a high- or low-intensity pain stimulus delivered to the left hand (Fig. 1a) (see Methods). Subjects were told that they were performing a study of reaction times and were asked to judge whether the cues appeared on the left or on the right side of a display monitor. The second cue in each sequence was fully predictive of the strength of the subsequently experienced pain; however, the first cue only allowed a probabilistic prediction. Thus, in a small percentage of

©2004 Nature Publishing Group

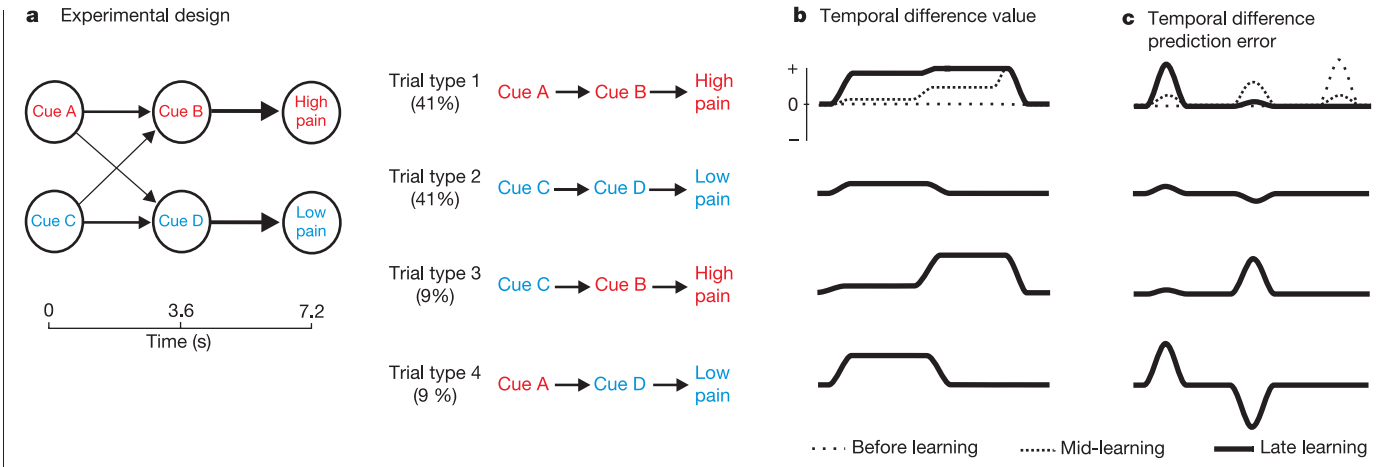

Figure 1 Experimental design and temporal difference model. **a**, The experimental design expressed as a Markov chain, giving four separate trial types. **b**, Temporal difference value. As learning proceeds, earlier cues learn to make accurate value predictions (that is, weighted averages of the final expected pain). **c**, Temporal difference prediction error; during learning the prediction error is transferred to earlier cues as they acquire the ability to make predictions. In trial types 3 and 4, the substantial change in prediction elicits a large positive or negative prediction error. (For clarity, before and mid-learning are shown only for trial type 1.)

trials, the expectation evoked by the first cue would be reversed by the second. This allowed us to study the neural implementation of both the expectations themselves, and their reversals.

Two important aspects of most accounts of prediction learning are the predictions themselves (termed values) and the errors in those predictions[9]. Figure 1b shows the predictions associated with each of the trial types 1–4. These predictions are calculated and revised as new stimuli are presented. Figure 1c shows the associated prediction error. The nature of this signal, which treats ongoing changes in predicted values on an exact par with actual affective outcomes, has helped to explain data on dopamine cell activity. This prediction error signal drives learning by specifying how the predictions should change. In appetitive conditioning the dopamine projection to the ventral striatum is believed to be a critical substrate for this signal, although apart from theoretical speculations about opponent processing[16], the equivalent for aversive conditioning is less clear. As in earlier work on appetitive conditioning, we used the temporal difference model to generate regressors based on the values and prediction errors appropriate to each individual subject[13]. Statistical parametric mapping of the regression coefficients permits identification of regions associated with, and in receipt of, information about predictions. Indeed, the temporal difference value was (negatively) correlated with the reaction times across subjects for the high-valued cues ($P < 0.001$), even when considering the second-order cue alone ($P < 0.01$). This result provides strong evidence that behavioural reinforcement occurs in a manner consistent with the temporal difference model.

The prediction error was highly correlated with activity in both the right and the left ventral putamen (Fig. 2). Correlations were also noted in the right head of the caudate, the left substantia nigra, the cerebellum (bilaterally) and the right anterior insula cortex (Fig. 2). Figure 3 shows the estimated responses in the right ventral putamen. As the most straightforward model coupling prediction error to BOLD signal would predict, positive (Fig. 3a) and negative (Fig. 3b) prediction errors at various times in the trial are clearly represented, as is the biphasic form of the prediction error (Fig. 3c).

We also investigated the representation of the temporal difference value (combining the predicted and the actual pain value, for reasons of analysis) by including the temporal difference value term in our regression model. This revealed correlated activity in the right anterior insula cortex (Fig. 4a). The estimated response is illustrated in Fig. 4c. The importance of this structure in pain learning has previously been identified[5]. In addition, we found temporal difference value-related responses in the brainstem (Fig. 4b). Precise anatomical localization of brainstem activation is difficult with standard neuroimaging, although we note a consistency with the probable location of the dorsal raphe nucleus. We also observed temporal difference value-related responses in the anterior cingulate cortex and the right amygdala, which did not survive statistical correction for multiple comparisons.

The striking resemblance between the BOLD signal in the ventral putamen and the temporal difference prediction error (Fig. 3) offers powerful support for the temporal difference model, in particular because this is a second-order paradigm. Other dynamic models of

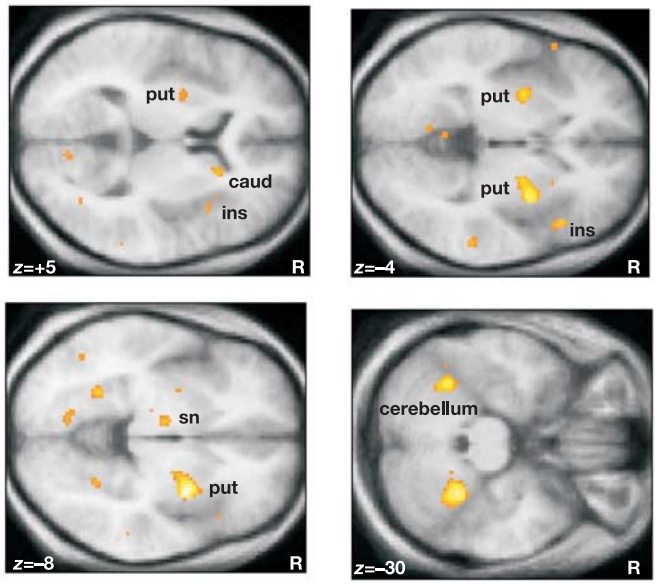

Figure 2 Temporal difference prediction error (statistical parametric maps). Areas coloured yellow/orange show significant correlation with the temporal difference prediction error. Yellow represents the greatest correlation. Peak activations (MNI coordinates and statistical *z* scores) are: right ventral putamen (put; (32, 0, −8), $z = 5.38$); left ventral putamen (put; (−30, −2, −4), $z = 3.93$); right head of caudate (caud; (18, 20, 6), $z = 3.75$); left substantia nigra (sn; (−10, −10, −8), $z = 3.52$); right anterior insula (ins; (46, 22, −4), $z = 3.71$); right cerebellum ((28, −46, −30), $z = 4.91$); and left cerebellum ((−34, −52, −28), $z = 4.42$). R indicates the right side.

©2004 Nature Publishing Group

pavlovian conditioning, such as the SOP models, do not involve this signal[17]. Our result adds to the growing body of neural and psychological data supporting the biological basis of temporal difference theory. In a framework called the actor–critic model for instrumental conditioning (and some variants)[18,19], the same prediction error signal is also used to train stimulus–response habits (called policies), ultimately leading to the choice of best possible actions[20]. Again, this has been much more intensively studied from the perspective of appetitive than aversive conditioning. Importantly, the higher-order process demonstrated here is a crucial substrate for learning in the changing and uncertain conditions that characterize real environments, and in principle is capable of supporting complex behaviours.

Our findings add to the existing pharmacological, electrophysiological, functional imaging and clinical evidence for the involvement of the striatum in aversive processing and learning[21]. Given that the BOLD signal in the same region is correlated with the temporal difference prediction error for rewards[13,15], this structure may advance our understanding of precisely how aversive and appetitive information are integrated to produce motivationally appropriate behaviour in the light of (predictions of) both.

At present, the nature of the phasic aversive prediction error signal is not clear. Substantial psychological data suggest the existence of separate appetitive and aversive motivational systems that act as mutual opponents over a variety of time courses[22,23]. Given the (not unchallenged[24]) suggestion that dopamine neurons in the ventral tegmental area and in the substantia nigra report appetitive prediction error, it has been suggested that serotonin-producing neurons of the dorsal raphe nucleus, which send strong projections to the ventral striatum[25], may encode aversive prediction error[16]. We show prediction-related responses in an area that incorporates this nucleus. There is an active debate about the involvement of dopamine in aversive conditioning[26,27], and an alternative possibility is that dopamine reports both aversive and appetitive prediction errors.

Our findings have important implications for our understanding of human pain, given that substantial evidence indicates that the experience of pain is modified by prior conditioning[28]. Here we show regionally distinct neuronal responses, consistent with established computational processes, providing a mechanism through which the affective and motivational aspects of pain can be modulated. □

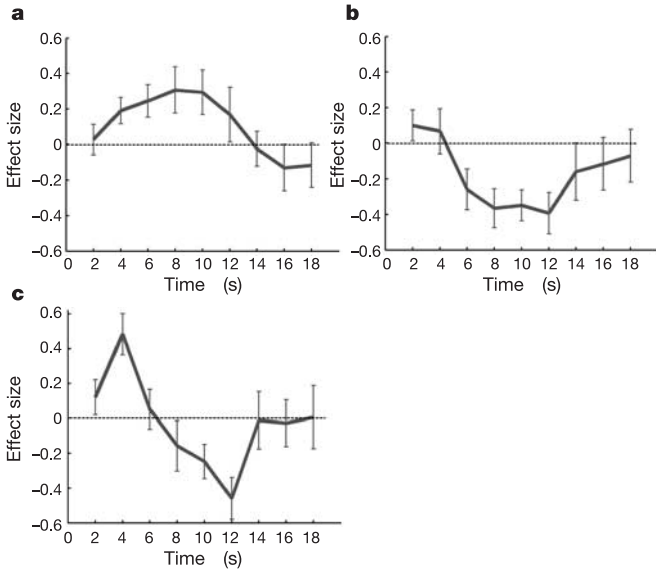

Figure 3 Temporal difference prediction error (impulse responses). Time course of the impulse response (±s.e.m.) to higher-order prediction error in the right ventral putamen. **a**, Positive prediction error (contrast of trial types 3 and 2). **b**, Negative prediction error (contrast of trial types 4 and 1). **c**, Biphasic prediction error; positive at the first cue, becoming negative at the second (contrast of trial types 4 and 2).

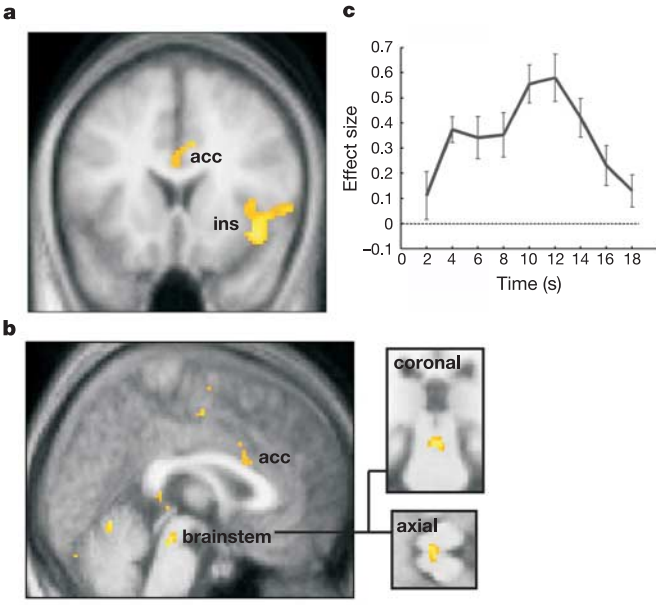

Figure 4 Temporal difference value (statistical parametric maps and impulse response in the right anterior insula). **a**, **b**, Areas showing significant correlation with the temporal difference value. Peak activations (MNI coordinates and statistical z scores) are: right anterior insula (ins; (42, 16, −14), $z = 4.16$); brainstem ((0, −28, −18), $z = 3.89$); and anterior cingulate cortex (acc; (8, 12, 32), $z = 3.82$). Coronal and axial slices of brainstem activation are shown, highlighting localization to dorsal raphe nucleus. **c**, Time course of impulse response (±s.e.m.) in right anterior insula cortex, from contrast of trial types 1 and 2.

Methods

Subjects and stimuli

The study was approved by the local ethics committee. Pain was delivered to the left hand by means of two silver chloride electrodes, using a 100-Hz train of electrical pulses (4-ms square waveform, 1-s duration). A variation of current amplitude (0.5–6.0 mA) was used to deliver high- or low-intensity stimuli, set on an individual basis; mean intensity ratings were 2.9 for low intensity and 8.0 for high intensity, on a 10-point scale. Post-experiment debriefing showed no evidence of habituation or sensitization. The visual cues were abstract coloured pictures, visible on a screen by means of a head coil mirror and presented to the left or right of (and above or below) the centre. Different cues were used for the two sessions, and fully counter-balanced.

The experiment

Each subject undertook two sessions, each representing a complete learning experiment consisting of 110 trials. In each trial two cues were presented in sequence (for 3.6 s each) followed immediately by a pain stimulus. Trials were separated by a randomized variable delay of mean 5 s (range 3.5–6.5 s). The probabilistic architecture defined in Fig. 1a gives four trial types, with types 1 and 2 occurring frequently (and solely for the first ten trials). Subjects reported the position of the cue (left or right) as quickly as possible by pressing a key, and were not told that the experiment was a learning task. Post-experiment debriefing showed that no subjects were fully aware of all cue–outcome contingencies, although the influence of awareness was not specifically addressed.

Temporal difference model

The sequence of cue and pain stimuli for each subject was entered into the temporal difference learning model: TD(0)[9] with no eligibility trace or discount factor, and on a trial basis. Each trial had three time points: first cue, second cue and pain stimulus. The six resulting states (s) were defined by the stimulus present at that time, each having a corresponding predictive value $V(s)$ (with an initial value of zero) and a return, r, representing the pain ($r = 1$ for the high intensity and $r = 0$ otherwise). At each point in time, t, the prediction error, δ, was defined as $\delta = r + V(s_t) - V(s_{t-1})$; that is, the difference between successive value predictions.

The previous state value predictions were then updated according to the algorithm $V(s) \leftarrow V(s) + \alpha\delta$, where α is the learning rate.

©2004 Nature Publishing Group

Data acquisition and analysis

We acquired T2*-weighted echo planar imaging (EPI) images with BOLD contrast on a 1.5 tesla Siemens Sonata magnetic resonance scanner (imaging parameters: 280 volumes; 2 mm slice thickness; 1 mm inter-slice gap; tilted plane acquisition sequence[29]). T1-weighted structural images were co-registered with mean EPI images, and averaged across subjects to allow group level anatomical localization.

Images were analysed using the statistical parametric mapping software SPM2. Preprocessing consisted of spatial realignment, normalization to a standard EPI template, and spatial smoothing with an 8 mm (full-width at half-maximum) gaussian kernel. Images were then analysed in an event-related manner. Stimuli were encoded as δ-functions and multiplied by the temporal difference prediction error at each event provided by the computational model for each subject, and then convolved with a canonical haemodynamic response function (HRF). The parameter estimates (that is, regression coefficients) were taken to a second level random effects group analysis using a one-way analysis of variance.

Group level SPMs were initially given a threshold of $P < 0.001$, uncorrected (as shown in Figs 2 and 4). To correct for multiple comparisons, we used 8 mm radius small volume corrections (reporting family-wise error correction at $P < 0.05$) in our areas of interest, based on data from previous investigations in our laboratory[30] (ventral putamen, anterior insula, anterior cingulate, amygdala and cerebellum). Areas in substantia nigra (Montreal Neurological Institute (MNI) coordinates ±10, −14, −10), upper brainstem (0, −26, −20) and dorsal striatum (±12, 14, 3) were anatomically defined from our mean structural image.

We report results using a learning rate of $\alpha = 0.5$. An approximate Taylor expansion of the prediction error at $\alpha = 0.5$ and calculation of SPMs of the appropriate F-test, suggested that this was near optimal, as did results from $\alpha = 0.2$ and $\alpha = 0.8$.

Impulse responses (Figs 3 and 4b) were characterized by supplementary analysis using a flexible basis set of 2-s duration finite impulse responses on a trial basis (removing the first ten trials of early learning). Time courses shown are the averaged estimated impulse responses for each trial (with the areas of interest defined on a subject-specific basis from the original temporal difference analysis).

The sum of the temporal difference and pain values (that is, 0 or 1) were incorporated for analysis of temporal difference value (given that our design is not optimal for distinction of the two), treating prediction error and pain as effects of no interest. We applied a mask (at $P < 0.05$, uncorrected) of areas showing significant increases in activity in the cue periods from the finite impulse response analysis to ensure identification of purely predictive areas.

We normalized the reaction times (excluding those greater than 1,500 ms) using cumulative distribution functions of individually fitted gamma-distributions and regressed these values on the temporal difference value for the high pain-predicting cues. In addition to the highly significant ($P < 0.001$) regression pooled over subjects, 8 out of 14 subjects showed individually significant correlations ($P < 0.05$), but no significant fMRI differences.

Received 2 December 2003; accepted 19 April 2004; doi:10.1038/nature02581.

1. Sutton, R. S. & Barto, A. G. in *Learning and Computational Neuroscience: Foundations of Adaptive Networks* (eds Gabriel, M. & Moore, J.) 497–537 (MIT, Cambridge, Massachusetts, 1990).
2. Everitt, B. J. *et al.* Associative processes in addiction and reward. The role of amygdala–ventral striatal subsystems. *Ann. NY Acad. Sci.* **877,** 412–438 (1999).
3. LeDoux, J. Fear and the brain: where have we been, and where are we going? *Biol. Psychiatry* **44,** 1229–1238 (1998).
4. Buchel, C. & Dolan, R. J. Classical fear conditioning in functional neuroimaging. *Curr. Opin. Neurobiol.* **10,** 219–223 (2000).
5. Ploghaus, A. *et al.* Dissociating pain from its anticipation in the human brain. *Science* **284,** 1979–1981 (1999).
6. Ploghaus, A. *et al.* Learning about pain: the neural substrate of the prediction error for aversive events. *Proc. Natl Acad. Sci. USA* **97,** 9281–9286 (2000).
7. Dickinson, A. *Contemporary Animal Learning Theory* (Cambridge Univ. Press, Cambridge, UK, 1980).
8. Sutton, R. S. & Barto, A. G. Toward a modern theory of adaptive networks: expectation and prediction. *Psychol. Rev.* **88,** 135–170 (1981).
9. Sutton, R. S. & Barto, A. G. *Reinforcement Learning: An Introduction* (MIT, Cambridge, Massachusetts, 1998).
10. Montague, P. R., Dayan, P. & Sejnowski, T. J. A framework for mesencephalic dopamine systems based on predictive Hebbian learning. *J. Neurosci.* **16,** 1936–1947 (1996).
11. Schultz, W., Dayan, P. & Montague, P. R. A neural substrate of prediction and reward. *Science* **275,** 1593–1599 (1997).
12. Suri, R. E. & Schultz, W. Temporal difference model reproduces anticipatory neural activity. *Neural Comput.* **13,** 841–862 (2001).
13. O'Doherty, J. P., Dayan, P., Friston, K., Critchley, H. & Dolan, R. J. Temporal difference models and reward-related learning in the human brain. *Neuron* **38,** 329–337 (2003).
14. Friston, K. J., Tononi, G., Reeke, G. N. Jr, Sporns, O. & Edelman, G. M. Value-dependent selection in the brain: simulation in a synthetic neural model. *Neuroscience* **59,** 229–243 (1994).
15. McClure, S. M., Berns, G. S. & Montague, P. R. Temporal prediction errors in a passive learning task activate human striatum. *Neuron* **38,** 339–346 (2003).
16. Daw, N. D., Kakade, S. & Dayan, P. Opponent interactions between serotonin and dopamine. *Neural Netw.* **15,** 603–616 (2002).
17. Brandon, S. E., Vogel, E. H. & Wagner, A. R. Stimulus representation in SOP: I. Theoretical rationalization and some implications. *Behav. Processes* **62,** 5–25 (2003).
18. Barto, A. G., Sutton, R. S. & Anderson, C. W. Neuronlike elements that can solve difficult learning problems. *IEEE Trans. Syst. Man Cybern.* **13,** 834–846 (1983).
19. Barto, A. G., Sutton, R. S. & Watkins, C. J. C. H. in *Learning and Computational Neuroscience: Foundations of Adaptive Networks* (eds Gabriel, M. & Moor, J.) 539–602 (MIT, Cambridge, Massachusetts, 1990).
20. Barto, A. G. in *Models of Information Processing in the Basal Ganglia* (eds Houk, J. C., Davis, J. L. & Beiser, D. G.) 215–232 (MIT, Cambridge, Massachusetts, 1995).
21. Chudler, E. H. & Dong, W. K. The role of the basal ganglia in nociception and pain. *Pain* **60,** 3–38 (1995).
22. Solomon, R. L. & Corbit, J. D. An opponent-process theory of motivation. I. Temporal dynamics of affect. *Psychol. Rev.* **81,** 119–145 (1974).
23. Dickinson, A. & Dearing, M. F. in *Mechanisms of Learning and Motivation* (eds Dickinson, A. & Boakes, R. A.) 203–231 (Erlbaum, Hillsdale, New Jersey, 1979).
24. Horvitz, J. C. Mesolimbocortical and nigrostriatal dopamine responses to salient non-reward events. *Neuroscience* **96,** 651–656 (2000).
25. Azmitia, E. C. & Segal, M. An autoradiographic analysis of the differential ascending projections of the dorsal and median raphe nuclei in the rat. *J. Comp. Neurol.* **179,** 641–667 (1978).
26. Mirenowicz, J. & Schultz, W. Preferential activation of midbrain dopamine neurons by appetitive rather than aversive stimuli. *Nature* **379,** 449–451 (1996).
27. Horvitz, J. C. Dopamine gating of glutamatergic sensorimotor and incentive motivational input signals to the striatum. *Behav. Brain Res.* **137,** 65–74 (2002).
28. Ploghaus, A., Becerra, L., Borras, C. & Borsook, D. Neural circuitry underlying pain modulation: expectation, hypnosis, placebo. *Trends Cogn. Sci.* **7,** 197–200 (2003).
29. Deichmann, R., Gottfried, J. A., Hutton, C. & Turner, R. Optimized EPI for fMRI studies of the orbitofrontal cortex. *Neuroimage* **19,** 430–441 (2003).
30. Buchel, C., Dolan, R. J., Armony, J. L. & Friston, K. J. Amygdala–hippocampal involvement in human aversive trace conditioning revealed through event-related functional magnetic resonance imaging. *J. Neurosci.* **19,** 10869–10876 (1999).

Acknowledgements We thank P. Allen and E. Featherstone for technical help. This work was funded by Wellcome Trust program grants to R.S.F., K.J.F., M.K. and R.J.D. P.D. was funded by the Gatsby Charitable foundation.

Competing interests statement The authors declare that they have no competing financial interests.

Correspondence and requests for materials should be addressed to B.S. (bseymour@fil.ion.ucl.ac.uk).

Myosin-dependent junction remodelling controls planar cell intercalation and axis elongation

Claire Bertet, Lawrence Sulak & Thomas Lecuit

Laboratoire de Génétique et de Physiologie du Développement (LGPD), Institut de Biologie du Développement de Marseille (IBDM), CNRS-INSERM-Université de la Méditerranée, Campus de Luminy, case 907, 13288 Marseille cedex 9, France

Shaping a developing organ or embryo relies on the spatial regulation of cell division and shape. However, morphogenesis also occurs through changes in cell-neighbourhood relationships produced by intercalation[1,2]. Intercalation poses a special problem in epithelia because of the adherens junctions, which maintain the integrity of the tissue. Here we address the mechanism by which an ordered process of cell intercalation directs polarized epithelial morphogenesis during germ-band elongation, the developmental elongation of the *Drosophila* embryo. Intercalation progresses because junctions are spatially reorganized in the plane of the epithelium following an ordered pattern of disassembly and reassembly. The planar remodelling of junctions is not driven by external forces at the tissue boundaries but depends on local forces at cell boundaries. Myosin II is specifically enriched in disassembling junctions, and its planar polarized localization and activity are required for planar junction remodelling and cell intercalation. This simple cellular mechanism provides a general model for polarized morphogenesis in epithelial organs.

Drosophila germ-band elongation (GBE)[3] leads to an almost doubling in length of the epithelial layer that forms the thorax and abdomen of the embryo (Fig. 1a, b). This extension is associated with a mediolateral convergence of cells along the dorsoventral (D/V) axis. Neither cell divisions nor changes in cell shape contribute to anteroposterior (A/P) axis elongation[3]; thus, GBE is solely

©2004 Nature Publishing Group